Thrust measurements using plasma pressure measurements in the plume: a feasibility

IEPC-2019-258

Presented at the 36th International Electric Propulsion Conference
University of Vienna • Vienna, Austria
September 15-20, 2019

Paul-Quentin Elias[1]
ONERA/DPHY, Université Paris Saclay, Palaiseau, France

Raphaël Levy
ONERA/DPHY, Université Paris Saclay, Châtillon, France

Julien Jarrige
ONERA/DPHY, Université Paris Saclay, Palaiseau, France

Vincent Gaudineau
ONERA/DPHY, Université Paris Saclay, Châtillon, France

and

Claude Boniface
CNES, Propulsion, Pyrotechnics and Aerothermodynamics department, Orbital systems directorate, Toulouse, France

Abstract: This work seeks to assess the feasibility of measuring the thrust of an electric thruster by measuring the plasma pressure in the plume. For this purpose, a thrust sensor is developed using highly-sensitive quartz micro-resonators as force sensors. The measurement methodology is exposed as well as the sensor design choices. The thrust sensor is characterized in the ONERA B61 vacuum chamber with a 50-W class ECR thruster. The biases affecting the sensor are identified. It is shown that the sensor is robust and sensitive enough for the measurement of the plasma pressure. Charge deposition and transient thermal drift perturbs the measurement in the current configuration. The changes needed to remove these effects are identified and will be implemented in a future design.

I. Introduction

The lifetime and performances drift of electric thrusters is primarily verified using ground qualification tests. In particular, these tests require periodical checks of the trust and beam divergence. The former is achieved by mounting the thruster on a thrust stand, the latter using electrostatic probes. While these methods are efficient and reliable, some test conditions prevent their use. For example, cold-start tests prevent the use of a thrust balance. For that reason, it would be desirable to obtain an independent mean to measure both the thrust and the beam divergence, without the constraints of the thrust balance.

One way to perform these combined measurements is to measure the force by probing the thruster plasma beam. Because of the momentum conservation, an integral measurement of the beam pressure yields the force applied by the plasma on the thruster, and thus gives the total thrust. The challenge is to measure a plasma pressure of a

[1] Corresponding author, paul-quentin.elias@onera.fr

few µN/cm2. ONERA designs and manufactures high-precision MEMS accelerometers, and this technology has been already transferred to industrial partners. Their unique design makes them usable as force sensor. Based on an ONERA proprietary technology, these miniature devices (< 1cm2) can reach sensitivities compatible with a direct measurement of the plasma pressure in the beam. The goal of this study is to assess the feasibility of this approach using these high-precision MEMS force sensors. For this purpose, the following actions have been performed:

- Theoretical analysis: a detailed analysis of the principles of the measurements has been performed, including the expected plasma pressure for a 50-W ECR thruster. The different perturbation factors have been quantified.
- Experimental study: a force sensor has been designed, manufactured and mounted next to an electrostatic probe in ONERA's B61 vacuum tank (fig 1). A 50-W class ECR thruster, mounted on a micro-newton thrust balance has been used as a reference thruster. This experiment has been used to assess the behavior and sensitivity of off-the-shelf quartz micro-sensors to perform force measurements (VIA type).

II. Pressure-based thrust measurement

A. Thrust measurement from a beam measurement

In this section, we derive the classical relationship between the thrust and the beam properties. To do so we make use of the momentum conservation equation, modified to include the contribution of the electromagnetic forces [1,2] :

$$\frac{\partial}{\partial t}(\rho\bar{V}+\epsilon\bar{E}\times\bar{B}) = -\nabla\cdot\left(\bar{\bar{T}}_M+\bar{\bar{T}}_{EM}\right) \tag{1}$$

Here $\bar{\bar{T}}$ is the momentum tensor given by:

$$\bar{\bar{T}}_M = \sum_\alpha \bar{\bar{P}}_\alpha + \rho_\alpha(\bar{V}_\alpha\otimes\bar{V}_\alpha) \tag{2}$$

And $\bar{\bar{T}}_{EM}$ is the Maxwell tensor:

$$\bar{\bar{T}}_{EM} = \frac{1}{2}\left(\epsilon_0 E^2+\frac{1}{\mu_0}B^2\right)\bar{\bar{I}} - \epsilon_0\bar{E}\otimes\bar{E} - \frac{1}{\mu_0}\bar{B}\otimes\bar{B} \tag{3}$$

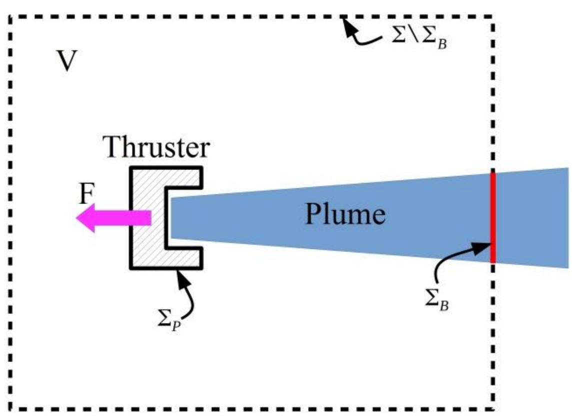

Figure 1 – Control surface enclosing the thruster and the near-field plume. The surface Σ_P encloses only the thruster. The section of Σ crossed by the plasma plume is noted Σ_B.

In a very general fashion[1], it can be shown that the thrust imparted by the plasma on the thruster is given by the integrated contribution of the total momentum (including the mass flux contribution $\bar{\bar{T}}_M\cdot\bar{n}$ and the electromagnetic contribution $\bar{\bar{T}}_{EM}\cdot\bar{n}$) on the thruster surface Σ_P :

$$\bar{F} = \int_{\Sigma_P}\left(\bar{\bar{T}}_M+\bar{\bar{T}}_{EM}\right)\bar{n}\,dS \tag{4}$$

For a steady state regime, the generalized momentum balance equation (1) is simply:

$$\nabla \cdot \left(\bar{\bar{T}}_M + \bar{\bar{T}}_{EM}\right) = 0 \tag{5}$$

Making use of the divergence theorem, one gets:

$$\int_V \nabla \cdot \left(\bar{\bar{T}}_M + \bar{\bar{T}}_{EM}\right) dV = 0 = \int_{\Sigma_P + \Sigma} \left(\bar{\bar{T}}_M + \bar{\bar{T}}_{EM}\right) \bar{n} dS = \bar{F} + \int_{\Sigma} \left(\bar{\bar{T}}_M + \bar{\bar{T}}_{EM}\right) \bar{n} dS \tag{6}$$

Hence:

$$\bar{F} = -\int_{\Sigma} \left(\bar{\bar{T}}_M + \bar{\bar{T}}_{EM}\right) \bar{n} dS \tag{7}$$

Surface Σ includes the whole system but the momentum fluxes and electromagnetic fields are only significant in a small portion Σ_B of that surface, where the plasma plume crosses Σ, has shown in Figure 1. The force applied by the plasma on the thruster can be simplified as:

$$\bar{F} = -\int_{\Sigma_{\mathrm{B}}} \left(\bar{\bar{T}}_M + \bar{\bar{T}}_{EM}\right) \bar{n} dS \tag{8}$$

This analysis show that the thrust can be obtained either by the integration of the generalized momentum flux on the thruster surface (4) or by integration of these same fluxes on a section of the plasma plume (8). The main idea of this work is to use the latter method. By using a very precise force sensor immersed in the thruster plume and integrating the measured profiles, one seeks to recover the total thruster imparted by the plasma on the thruster. The key point is to measure accurately and with as little perturbation as possible the momentum fluxes (i.e. the plasma pressure) in the beam. To do so a miniature force sensor is needed.

B. Quartz micro-resonator force sensors

The principle of the force sensor is shown in Figure 2. A test mass is mounted on a decoupling frame. The mass is maintained by two hinges and a narrow vibrating beam. A feedback circuit is used to excite the beam to its resonant frequency. When a force or acceleration is applied on the test mass, the tension through the vibrating beam changes and this shifts the resonant frequency.

The measurement of the resonant frequency of the vibrating beam provides an accurate measurement of the test mass acceleration (or the force applied on it). In fact, this technique provides a very stable measurement because of the inherent stability of the resonant frequency of the quartz crystal resonator.

These resonators are batch-manufactured using quartz wafers and chemical etching and photolithography which are precise and cost-effective manufacturing techniques. The ONERA micro-resonator design is particularly appropriate for plasma pressure measurement. Contrary to most MEMS accelerometers or force sensors, its measurement axis is perpendicular to the test mass and not in the crystal plane. In addition, its high sensitivity means that it can resolve the low force level imparted by the plasma on the test mass.

The sensor sensitivity is given the ratio between the resonant frequency and the acceleration imparted to the test mass:

$$K_1 = 1.5 \, \frac{hM}{e^2 ld\sqrt{E\rho}} \quad [\mathrm{Hz.\,g^{-1}}] \tag{9}$$

Here, as shown in Figure 2, E is the quartz Young modulus, ρ the volume mass of quartz, M is the mass of the test mass, e is the width of the vibrating part of the beam, l its non vibrating width, h is the distance between the test mass center of mass and the rotation axis, d is the distance between the beam and the hinges and e is the quartz wafer thickness. The typical single cell sensitivity is $K_1 = 12$ Hz.g^{-1}. If the sensor is used for surface force measurements, then its sensitivity is:

$$K_1 = 1.5 \times 10^{-3} \, \frac{hS}{e^2 ld\sqrt{E\rho}} \quad [\mathrm{Hz\,/\,\mu N.\,cm^{-2}}] \tag{10}$$

Where S is the surface of the test mass exposed to the force. Note that the sensitivity does not depend on the test mass in that case.

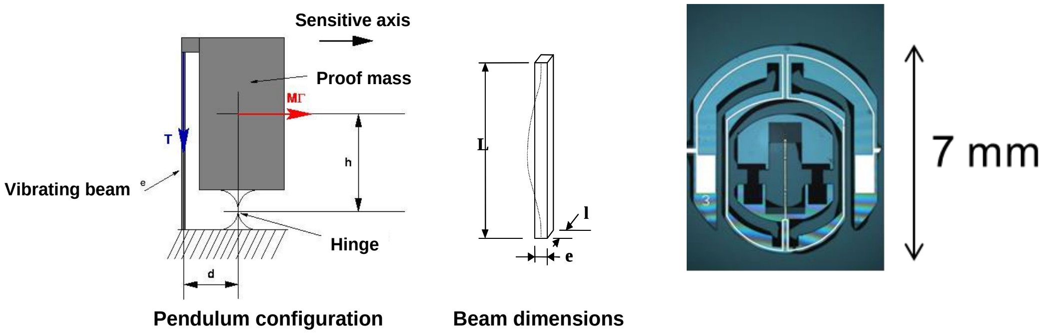

Figure 2 - Right: principle of operation of the vibrating accelerometer. Left: detailed view of VIA (Vibrating Integrated Accelerometer) cell.

C. Measurements scenario

The force measurement is performed by moving the sensor in the thruster plume. Angular scans of the plume are performed using a rotating arm holding a set of probes, including the force sensor, as shown in Figure 3.

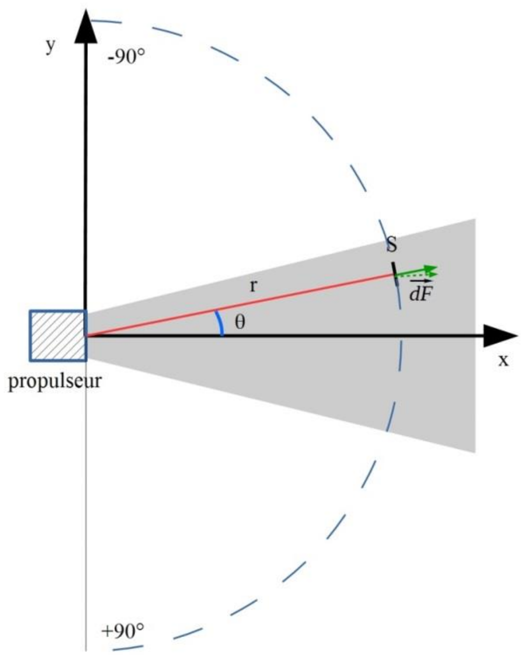

Figure 3- Probe coordinates for the beam angular scan

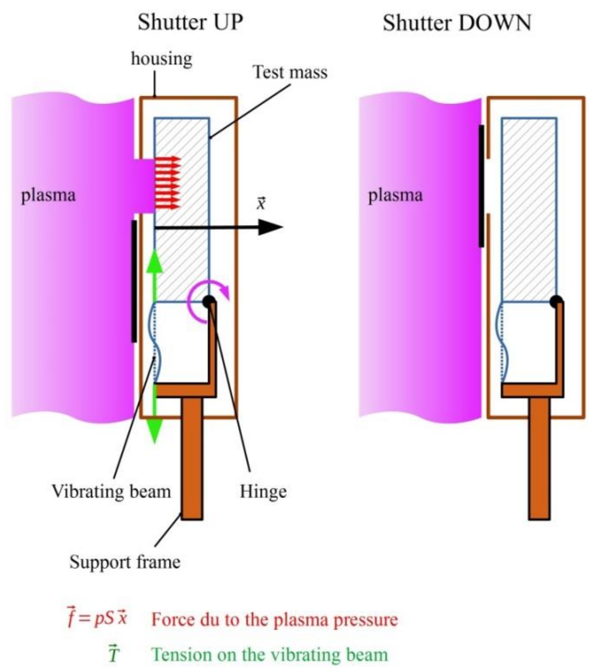

Figure 4 – Schematic view of the operation of the sensor in force measurement mode. When the shutter is opened, the plasma pushes on the test mass and changes the beam tension.

From the angular force profile, the thrust can be recovered. The biases due to the probe mounting tilt and the thermal drift can be compensated using a shutter that covers the force sensor, as shown in Figure 4. The shutter is closed to perform a reference measurement with no plasma at each position. This reference measurement includes the biases due to the current sensor tilt (which can change depending on the angular position) and the thermal load on the probe. When the shutter is opened, the frequency variation provides a measurement of the plasma pressure on the test mass.

Following equation (8), the thrust vector is given by integrating the momentum flux on a beam section Σ_B. If we define $\overline{dF} = \left(\bar{\bar{T}}_M + \bar{\bar{T}}_{EM}\right) \cdot \bar{n}$, the thrust is given by:

$$\bar{F} = -\int_{\Sigma_B} d\bar{F} \tag{11}$$

If the beam section is far from the thruster, the electromagnetic part of the momentum tensor becomes negligible. In this condition, the thrust component along the thruster axis is:

$$F_x = -\int_{\Sigma_B} \left(\sum_\alpha \bar{\bar{P}}_\alpha \bar{n} \cdot \bar{e}_x + \rho_\alpha V_n^\alpha V_x^\alpha \right) dS \tag{12}$$

In principle, the computation of the thrust force requires to measure the plasma pressure (in red in equation (12)) over the whole surface Σ_B. Experiments provide a sampling of this quantity over a discrete number of positions. If the beam is asymmetrical, then it is possible to limit the sampling to an angular profile, as shown in Figure 3. In this case Σ_B is a portion of a spherical shell

D. Analysis of the measurement biases

The measurement of the plasma pressure with the highly sensitive force sensor can be biased by several phenomena.

First, the plasma flux causes a thermal load on the force cell which heats up. This heating induces a drift of the resonance frequency of the vibrating beam. This known phenomenon can be compensated by using two cells to perform a differential measurement. This method rejects the common mode variation of the frequency due to the variation of the temperature. We use two identical cells with their measurement axis aligned but in opposite directions. If the cells are close enough, they experience the same plasma conditions, including the pressure and the heat flux. In these conditions, the first cell resonance frequency is given by[3] :

$$F_1 = F_{01} + K_1\Gamma + K_2\Gamma^2 + F(T) \tag{13}$$

Here, F_{01} is the oscillator resonant frequency (at rest), $K_1 = 12\ \mathrm{Hz.g^{-1}}$ is the linear sensitivity, K_2 is the quadratic sensitivity, Γ is the acceleration of the test mass and $F(T)$ is a function of the sensor temperature which models the thermal drift of the resonance frequency. For the second cell, whose measurement axis is aligned with the first one but with opposite direction, the oscillator frequency is:

$$F_2 = F_{02} - K_1\Gamma + K_2\Gamma^2 + F(T) \tag{14}$$

The differential measurement cancels out the thermal drift and the quadratic part of the frequency shift and double the measurement sensitivity:

$$\Delta f = F_1 - F_2 = 2K_1\Gamma \tag{15}$$

In the remainder of this paper, we will refer to Δf as the differential signal.

Second, the plasma flux on the test mass results in a charge deposition. The test mass is part of the quartz MEMS and has a very high resistivity. Any charge deposited on its surface will induce a force which is not a bias per se since it corresponds to an actual force. However this biases the plasma pressure measurement. As a first estimate we assume that the charges deposited on the test cell induce a floating voltage ΔU. These charges will be attracted to the grounded metal screen used to house the cell. The resulting pressure on the test is bounded by:

$$|\delta p_{ES}| \leq \frac{\varepsilon_0 \Delta U^2}{2d^2} \tag{16}$$

Where d is the distance between the cell and the metal housing and ε_0 is the dielectric permittivity in vacuum. Depending on the test mass resulting floating voltage ΔU, this bias might not need to be compensated. Initially it was assumed that the voltage would be of the same order of magnitude as the floating voltage measured on the probe, i.e. $\Delta U \leq 10$ V. In these conditions, the electrostatic bias is negligible.

Third, the slight misalignment of the rotating arm holding the probes might result in a slight tilt of the sensor with respect to the gravity. As a consequence, the local gravity vector may have a non-zero projection along the sensor measurement axis, as shown in Figure 5. This projection results in a bias in the measured force acting on the test mass. Fortunately this bias can be removed if reference measurements are available. These measurements are performed at the same angular position, but without the plasma pushing on the test mass. This can be achieved either with a shutter or with a reference measurement taken after the thruster cut off.

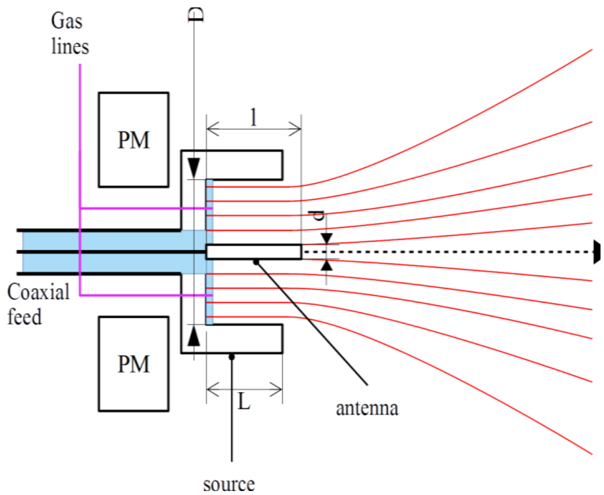

Figure 6 - Schematic view of the ECR thruster

III. Experiment setup

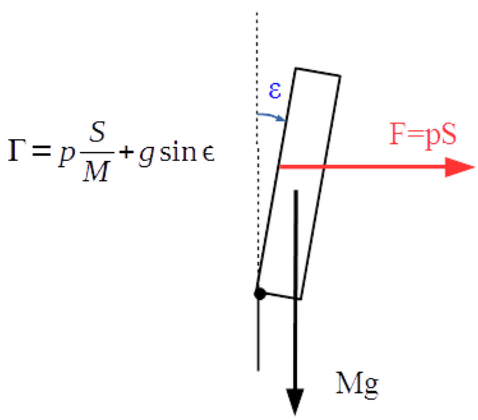

Figure 5 - Effect of the test mass misalignment with respect to the gravity vector

A. Vacuum tank

The tests were performed in ONERA's B61 vacuum tank (4 m in length, 1 m in diameter). This facility is equipped with a 2000 L/s turbopump and a cryopump, giving an overall pumping speed for Xenon of 8000 L/s. For this test the ultimate pressure was around $4 - 7 \times 10^{-7}$ mbar (in air). The background pressure with the thruster firing (0.1 mg/s xenon) was around 10^{-5} mbar.

B. Thruster

The tests were performed with a 50-W class permanent magnet ECR thruster developed at ONERA. Briefly, the thruster consisted in a coaxial source (diameter 27.4 mm, 20 mm in length), as shown in Figure 6. The inner conductor (antenna) was 2.3 mm in diameter. The coaxial chamber was fed by a custom 50 Ω coaxial line, two gas injection lines (1.1 mm in diameter). The static magnetic field was produced by a permanent magnet assembly (version PM1).

For these tests, the thruster was operated at a constant set point with a xenon mass flow of 0.1 mg/s and an incident input power around 30 W. Further details on the thruster characteristics and operation are provided in by Vialis et al. and Correyero et al. [4,5].

C. Diagnostics

The performances of the thruster were characterized using two types of diagnostics. Alongside the thrust sensor, a Faraday probe was used to measure the ion current density in the beam. The ECR thruster was mounted on one-axis thrust balance. Details on both of these diagnostics can be found in [4,6,7].

D. Thrust sensor

The thrust sensor is shown in Figure 7. Two VIA-class quartz cells were mounted on a copper plate. The sensor electronics, composed of a charge amplification stage and a feedback stage were mounted on the copper plate, as shown in Figure 8. An aluminum housing protected the electronic boards from the plasma. Two 0.5-mm thick metal covers were mounted in front of the quartz cells to protect the fragile parts of the cells. On each plate, two diaphragms were machined and centered just above the test mass of the underlying cell, as shown in Figure 9. Two sets of covers were available, one with diaphragms 0.6 mm in diameter, the other with diaphragms 1.0 mm in diameter. The resulting sensitivity for the sensor is shown in Table 1. A remote controlled shutter was mounted over the two cover plates. The shutter covers the diaphragms simultaneously, as shown in Figure 10.
Two temperature probes (Pt100) were mounted on the sensor: one was located inside, close to the upper quartz cell, as shown in Figure 8. The other was mounted in front of the sensor, as shown in Figure 10.
The conditioning electronics of the two cells were located in the thruster and required de +5V DC power supply. The measurement signals were two square wave signals (5V in amplitude) that were connected to two Agilent 53131A frequency counters. The frequency measurement has a resolution of 10 µHz.

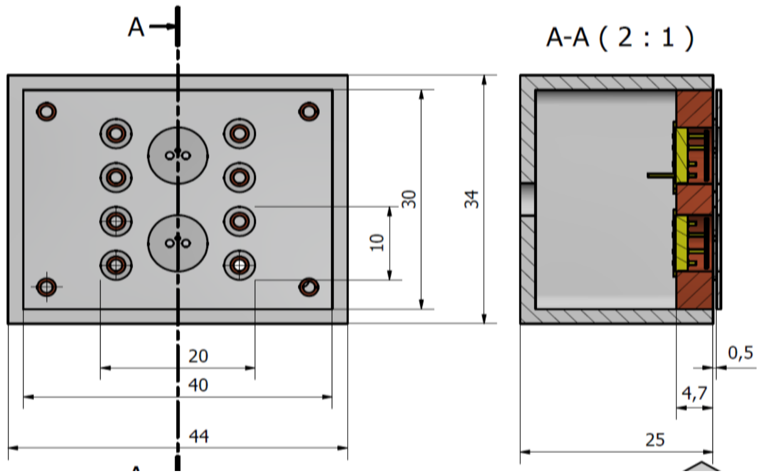

Figure 7 – CAD view of the sensor assembly, showing the housing and the copper mounting plate of the two VIA cells (in yellow). The conditioning electronics of both cells is located in the sensor assembly

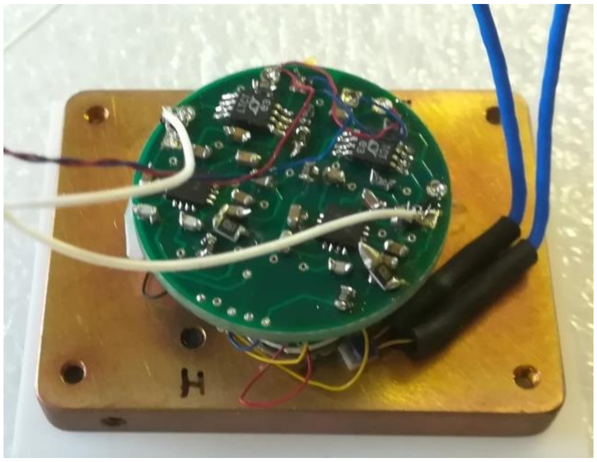

Figure 8 – View of the copper mounting plate and the conditioning electronics. A Pt100 temperature probe is mounted close to the upper cell to measure the internal temperature.

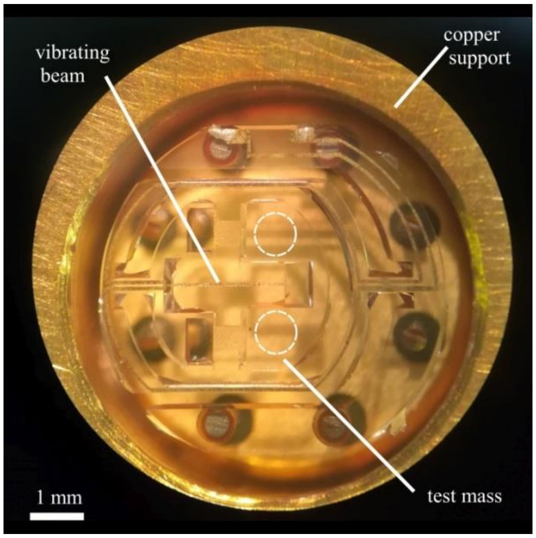

Figure 9 – View of a quartz cell mounted on the copper base plate. The cover plates mounted on top of the cell protect the sensitive parts of the cell. The two dashed circles outline the diaphragms.

Table 1 – Differential sensitivity of the thrust sensor.

Configuration	Cover plate diaphragms	Differential sensitivity
1	2 x Diam 0.6 mm	2 mHz / µN.cm^{-2}
2	2 x Diam 1.0 mm	5.5 mHz / µN.cm^{-2}

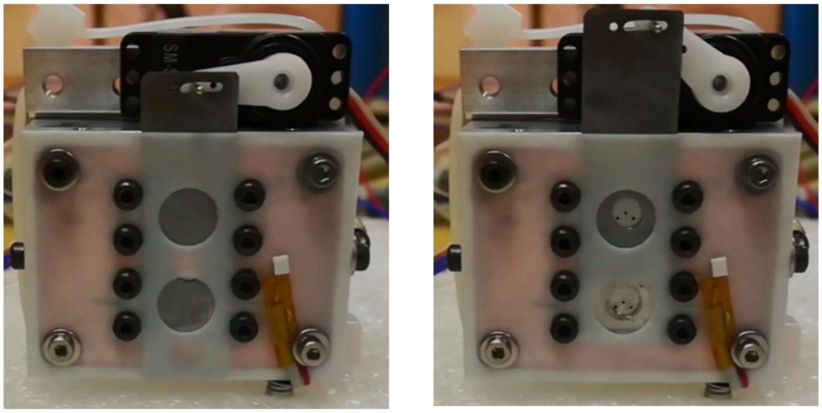

a) Shutter Closed *b) Shutter Opened*

Figure 10 –View of the two positions of the shutter. The external temperature probe can be seen on the right part of the sensor front face.

IV. Results

A. Thruster parameters

The same thruster set point was used for all the tests. Table 2 provides the main characteristics of the thruster. The set point was chosen such as to enable a stable operation of the thruster. The beam profile of the thruster is shown in Figure 11. This beam profile can be used to compute the expected plasma pressure, as shown in Figure 12. The plasma pressure to be measured ranged between 0.1 µN.cm^{-2} to 2 µN.cm^{-2}, well above the resolution limit of the sensor.

Table 2 – Thruster parameters

Parameter	Value
Xenon mass flow rate [mg.s^{-1}]	0,10
Absorbed power [W]	30±5
Thruster self-bias [V]	110±10
Ion energy [eV]	150±10
Thrust [µN]	450±10

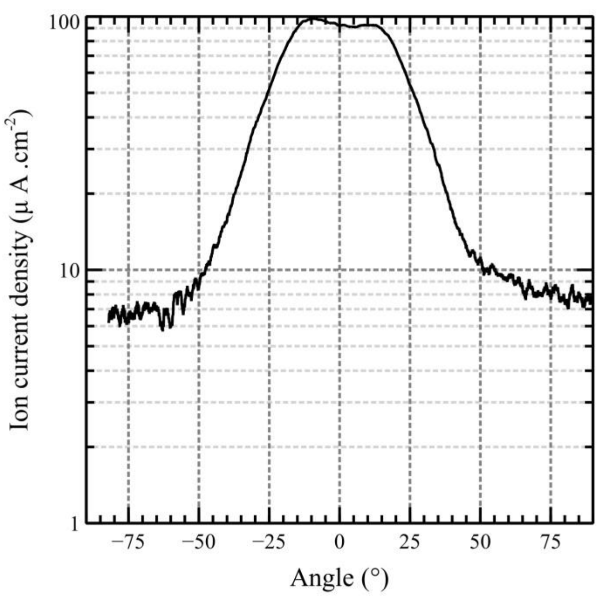

Figure 11 – Angular profile of the ion current density. Faraday probe distance L=150 mm from the thruster

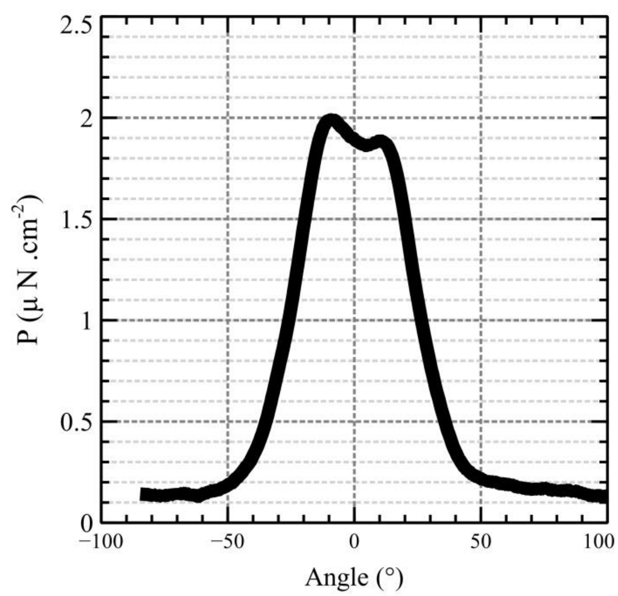

Figure 12 – Computed plasma pressure (150 mm from the thruster), with an ion energy Ei=150 eV.

B. No plasma case

For the test conditions described above, the expected differential signal shift due to the plasma is of a few millihertz. While the force sensor has a measurement resolution well below this level, several perturbations might prevent the detection of the plasma signal. In this section, the main sources of perturbation are experimentally quantified.

1. Thermal compensation

The thrust sensor uses two quartz cells to perform a differential measurement of the plasma pressure, as discussed in section II.D. The differential measurement rejects the thermal common mode frequency drift. The efficiency of this rejection can be seen in Figure 13. The rise of the sensor internal temperature is correlated with a significant drift of the resonant frequency of the two cells (~ 100 mHz). However, the differential signal Δf is nearly constant over the whole temperature range. The initial variation is due to the shutter movement, leading to an offset of ~ 10 mHz. After this transient, the differential signal drifts by 5 mHz at most (20 times less than a single cell frequency drift).

This demonstrates the efficiency of the thermal compensation. It is important to note that the differential measurement is effective if the two quartz cells experience the same plasma conditions (same heat load, same flux). This is true as long as the distance between the two cells is small compared to the characteristic variation length of the plasma in the plume.

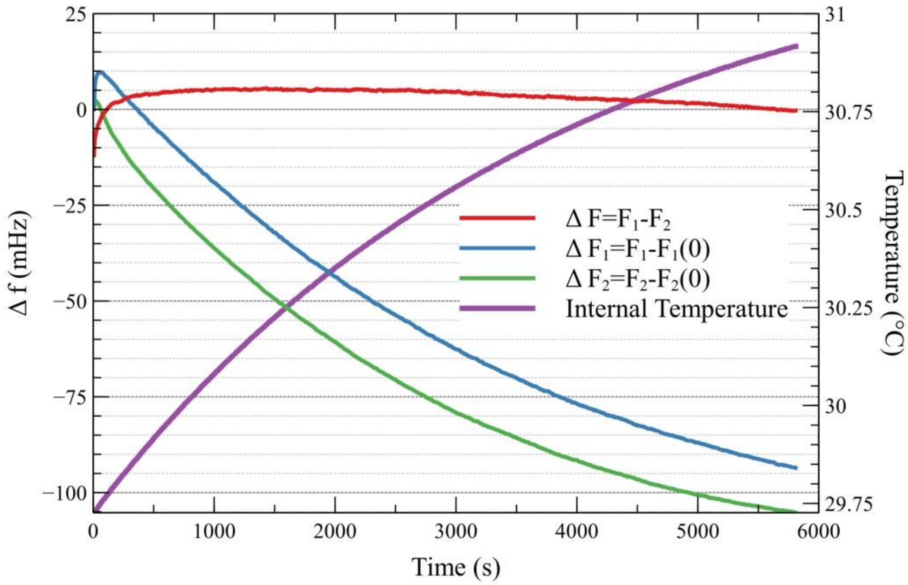

Figure 13 – Time evolution of the fundamental frequencies and the differential frequency during the sensor heat up. The shutter is opened at t=0 for 6000 s.

2. Repeatability

In Figure 14, the variation of the differential signal Δf during two angular scans is shown. The shift in frequency when the rotating arm angle is changed is due to a change the sensor tilt angle with respect to the gravity vector, as discussed in II.D. The two scans corresponds to the same angular sector but with opposite directions. The measurements of both scans are superimposed, which show the repeatability of the measurement. The lower graph in Figure 14 plots the difference between the two scans. This provides a good idea of the measurement repeatability between successive measurements. The standard deviation between of the shot-to-shot measurement is 1.6 mHz, below the thermal drift (5 mHz).

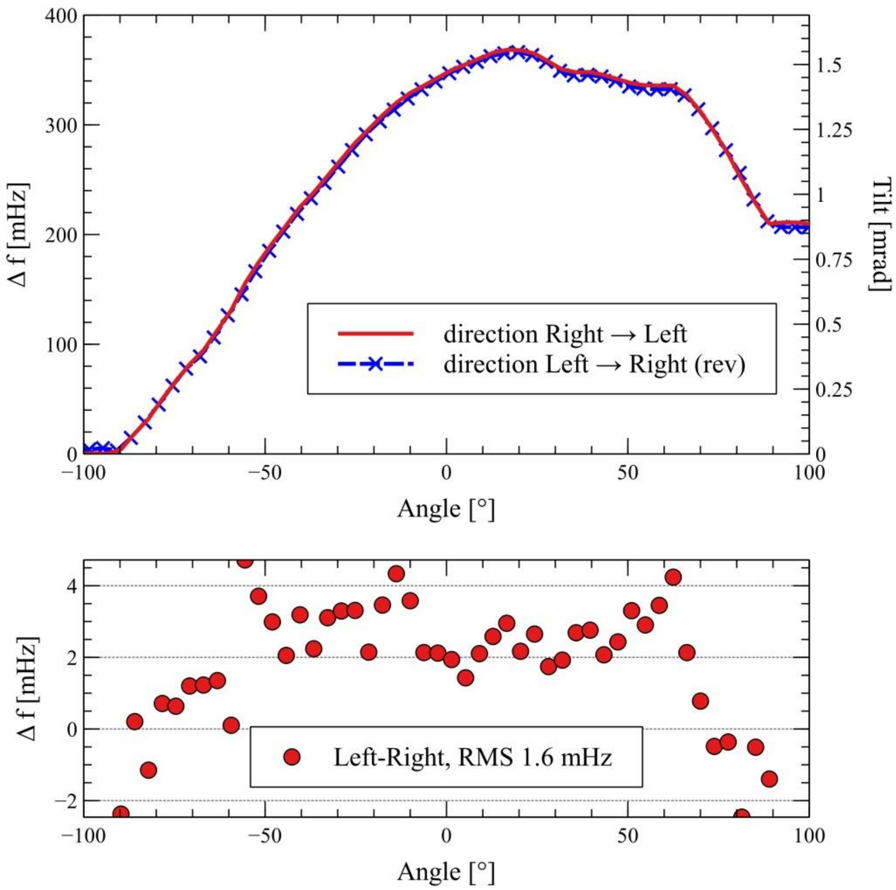

Figure 14 – Differential signal variations during an angular scan (right to left and left to right). The right axis on the upper graph gives the equivalent tilt angle, in milliradian. The lower graph gives the Δf variations between the two scans. Scan angular speed 2,5 °/s, sensor integration time 1s.

3. Shutter bias

The shutter transition time between the opened and closed position is less than 0.5 s. This movement causes a transient acceleration of the sensor which is seen as a force. It is necessary to compensate for this offset which bias the true measurement. To investigate this phenomenon, several sequences of 3 shutter cycles are performed, with different integration times for the frequency counter, as shown in Figure 15. Each transition of the shutter causes a reversible offset of the differential signal. Depending on the integration time, the offset is around 8-15 mHz. Except for the first transition for the smallest integration time, Figure 15 shows that the frequency offsets are very repeatable. This means that it is possible to compensate for the shutter-induced bias of the differential signal. The residual uncertainty resulting from this compensation is 0.5 mHz at most.

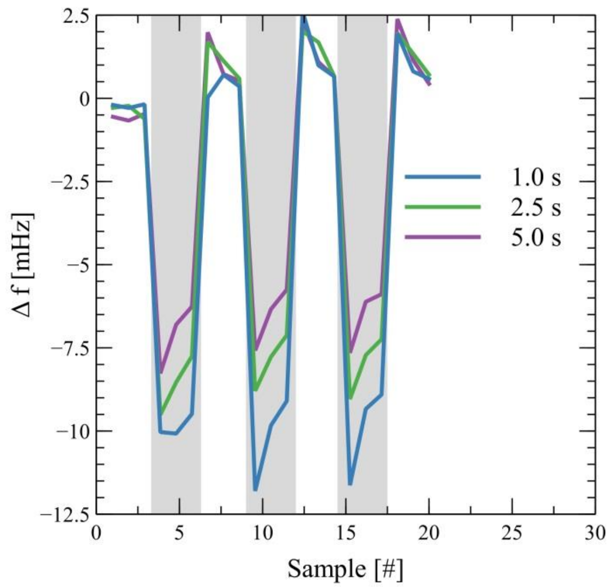

Figure 15 – Differential signal variations during three shutter cycles. The greyed areas mark the period when the shutter is opened.

C. Measurements in the plume

1. Angular scans

Angular scans performed in the plasma plume with the shutter in the open position shows that the oscillators become unstable when the sensor is close to the thrust axis, as shown in Figure 16. The resonant frequency of both cells increases by several tens of kilohertz when the angle is between -20° - 20°. An analysis of the oscillator signal in this angular range indicates that the square wave signal is frequency-modulated. This suggests that a secondary mode of the oscillators is excited and becomes dominant. This effect is directly correlated to the plasma exposition. Both oscillators recover their nominal frequency when the shutter is closed. It is possible that the plasma injected in the probe cavity causes stray currents that disturb the feedback loop of the oscillator. Unfortunately, the feedback circuit being hardwired inside the probe, it is not possible to change its gain to investigate further this effect. As a consequence, the remaining measurements are performed out of the thrust axis.

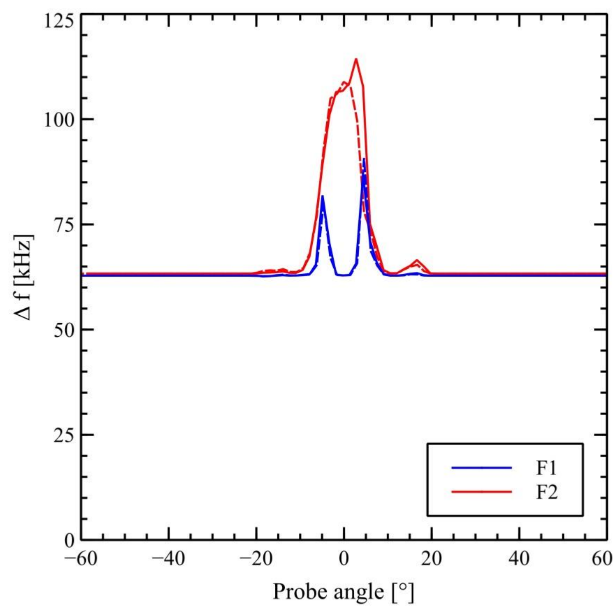

Figure 16 – Resonant frequency of the quartz cell as a function of the angular position (0° is the thruster axis), configuration 2, L=275 mm.

2. Measurement noise

For a static angular position where both cells respond nominally, the differential signal noise is compared between the plasma on and plasma off condition. For this purpose, the sensor is exposed to the plasma for 4 minutes, shutter open, repeatedly. The same sequence is performed with the thruster off, as shown in la Figure 17. Figure 18 compares the measurement noise in both situations. This noise is obtained by subtracting a linear trend to the signal which account for the drift of the sensor over the 4 minutes (thermal drift). When the plasma is off, the signal noise figure is around 0.3 mHz. The noise amplitude increases by a factor 6 to 7, up to 2 mHz, when the plasma is turned on. A possible cause for this increase is the electromagnetic noise radiated by the plasma. This 2 mHz noise provides the lower resolution limit of the current thrust sensor.

3. Fixed point measurements

Fixed point measurement in Figure 17 show that the pattern of repeated exposure to the plasma appears clearly in the differential signal Δf. The signal drops significantly (~150-200 mHz) when the shutter is opened in the plasma plume. When the cells are exposed to the plasma, the differential signal remains relatively constant, with a drift compatible with a thermal drift. When the shutter is closed, the differential signal rises sharply. The amplitude of the signal drop is consistent with an increase of the pressure applied on the test mass by ~ 15-30 µN.cm^{-2}. However, when the current density profile of the thruster and the ion energy is used to estimate the expected plasma pressure, it appears that for the current angular position the plasma pressure should be in the 0.1-0.2 µN.cm^{-2} range. The measured signal is two orders of magnitude above the expected one.

In addition, the differential signal shows a significant drift when the shutter is closed. As explained above the signal is nearly constant when the cells are exposed to the plasma. When the shutter cover the cells, the signal increases by 100-150 mHz in less than 1 s. Then it keeps on increasing by roughly another 100 mHz in a few tens of seconds. During this phase, the internal temperature of the sensor is nearly constant. A closer examination of the frequencies of both quartz cells indicates that this drift can be seen as a slowly evolving force pulling on the test mass.

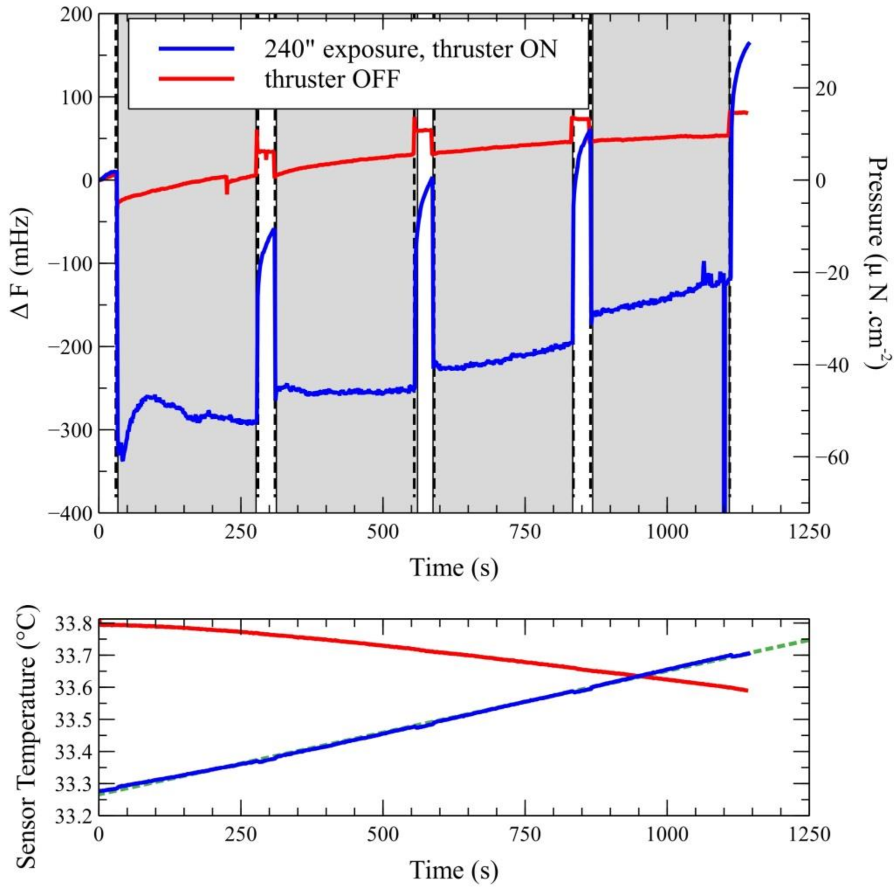

Figure 17 – Sequence of 4' exposure of the sensor, with the thruster on (blue) and off (red). The greyed areas indicate the period when the sensor is exposed (shutter open). The sensor is located 155 mm from the thruster, angle $\theta = 70°$ *integration time 0.5 s, configuration 2.*

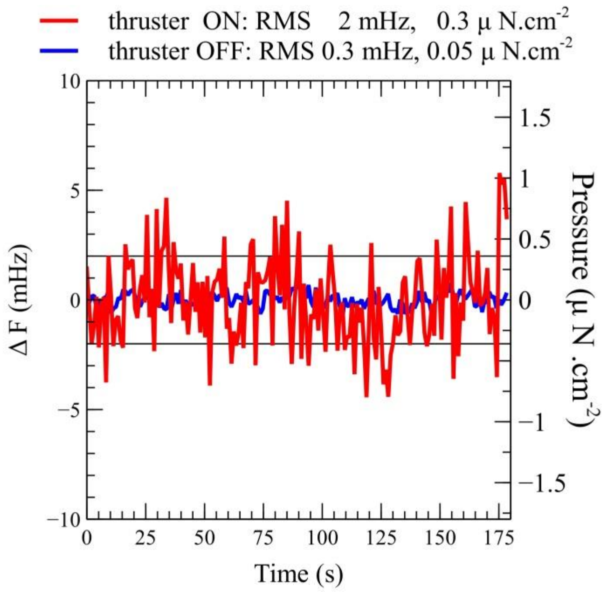

Figure 18 – Differential signal measurement noise with the plasma on and off, shutter open.

D. Discussion & perspective

The experimental tests of the thrust sensor in the plume have resulted in the following findings:

- The oscillating circuit becomes unstable when the sensor is located close to the thrust axis. It is possible that the residual plasma in the probe detune the feedback circuit. It was not possible to change the hardwire feedback loop, therefore the measurement where limited to off axis positions axe (|θ|>40°).
- The RMS noise of the sensor exposed to the plasma is 2 mHz, compared to 0.3 mHz when the shutter is closed.
- When the shutter is opened, a significant drop in the differential signal is recorded. The amplitude of this drop (~ 100-200 mHz) is well above the expected drop (a few mHz) for the plasma pressure expected.
- The differential signal is relatively stable when it is exposed to the plasma. It drifts significantly when the shutter is closed. This drift can be attributed to a force acting on the test mass.

Because of these phenomena, it has not been possible to obtain a reliable plasma pressure measurement with the current setup. However, these findings provide the guideline to improve the sensor. The first two points suggest that the current experimental setup is too sensitive to the plasma induced EMC. Therefore, the improved setup should shield the electronics more effectively and allow for hot-tuning of the feedback electronics. The two last points can be interpreted as the results of two possible causes:

1. Accumulation of residual charges on the test mass. In fact the quartz is a very good insulator. When the shutter is opened, the plasma can deposit charges on the test mass. This charge is normally shielded by the plasma. When the shutter is closed, the shielding disappears. Since there is no mechanism to drain the surface charge, this induces an electrostatic force that pulls on the test mass.
2. The thermal load induced by the plasma flux on the test mass can cause slight temperature gradients in the test mass. These gradients can cause a differential thermal expansion in the quartz frame that result in a stray force on the test mass.

While it is currently not possible to decide which hypothesis is more appropriate, these two possible causes also suggest a way forward for an improved setup. An improved device should provide a way to drain the charges accumulated on the test mass. In addition, it should provide a way to dampen the effect of a temperature gradient.

V. Conclusion

In summary, this work has examined the feasibility of performing beam force measure to measure the thrust of an electric thruster. For this purpose, a thrust sensor has been developed, based on highly-sensitive quartz cell developed by ONERA. This sensor uses two cells in differential mode to measure the plasma pressure in the thruster plume. A theoretical analysis has shown that it is possible to recover the thrust from a sampling of the plasma pressure in a section of the plume. Static tests have been performed in the plume and have shown that:

- The sensor is robust and sufficiently sensitive to achieve the desired measurement accuracy
- The measurements show a good repeatability. The biases due to the mechanical setup (tilt angle, shutter noise) can be efficiently compensated
- Measurement in the plasma shows that the sensor electronics is perturbed by the plasma when the sensor is too close the thrust axis. However, a force can be measured when the sensor is off-axis. Its magnitude is two orders of magnitude above the expected

The findings of this feasibility study are very encouraging. While no direct measurement has been achieved, these results points towards an improved experimental setup. This research will be pursued with an improved sensor that will build on these findings and will make use of another class of optimized quartz cell.

Acknowledgments

This work has been funded through the CNES grant R&T R-S18/PF-0005-107.

References

1. Nasi, L. & Raimbault, J.-L. A generalization of the rocket formula and its application to advanced space propulsion systems. *Acta Astronaut.* **68**, 34–38 (2011).
2. Giordano, D. Hypersonic-Flow Governing Equations with Electromagnetic Fields. *33rd Plasmadynamics Lasers Conf.* 1–28 (2002). doi:10.2514/6.2002-2165
3. Janiaud, D., Le Traon, O., Muller, S. & Bouniol, P. Accéléromètre à lames vibrantes de classe inertielle VIA. in *Symposium international : missles tactiques* (1998).
4. Vialis, T., Jarrige, J. & Packan, D. Direct Thrust Measurement of ECR plasma Thruster Performance and Comparison between Xenon and Krypton. in *35th International Electric Propulsion Conference* IEPC-2017-378 (2017).
5. Correyero, S., Jarrige, J., Packan, D. & Ahedo, E. Measurement of Anisotropic Plasma Properties along the Magnetic Nozzle Expansion of an Electron Cyclotron Resonance Thruster. in *35th International Electric Propulsion Conference* IEPC-2017-437 (2017).
6. Vialis, T., Jarrige, J., Aanesland, A. & Packan, D. Direct Thrust Measurement of an Electron Cyclotron Resonance Plasma Thruster. *J. Propuls. Power* **34**, 1323–1333 (2018).
7. Vialis, T. Développement d' un propulseur plasma à résonance cyclotron électronique pour les satellites. (Sorbonne Université, 2018).